Influence of velocity on conductor casing driving via Material Point Method

Raniel D. A. Albuquerque[1], Juliana S. Baioco[1], Breno P. Jacob[1], Jennifer M. F. Melo[2], Beatriz R. Barboza[2], João P. L. Santos[2], Mávyla S. C. Tenório[2], Fábio S. Cutrim[3], Rafael Dias[3]

[1]*COPPE, Federal University of Rio de Janeiro*
Cidade Universitária, 21941-901, Rio de Janeiro, Brazil
raniel.albuquerque@coc.ufrj.br, jsbaioco@lamcso.coppe.ufrj.br, breno@lamcso.ufrj.br
[2]*Laboratory of Scientific Computing and Visualization, Federal University of Alagoas*
Cidade Universitária, 57072-970, Alagoas, Brazil
jennifer.ferreira@lccv.ufal.br, mavyla.tenorio@lccv.ufal.br, beatriz@lccv.ufal.br, jpls@lccv.ufal.br
[3]*Petrobras*
Edifício Senado. Rua Henrique Valadares, 20231-030, Rio de Janeiro, Brazil
fabiosawada@petrobras.com.br, rafael_dias@petrobras.com.br

Abstract. The conductor is the first casing installed in an oil well, and it has important functions regarding the reliability of the initial phase of well construction. The soil response to the conductor installation is an important factor, as poor installation may cause excessive wear on the wellhead equipment or even result in the loss of the well. Therefore, a simulation of the self-weight phase of conductor driving was conducted to enhance knowledge about the soil's state during this process. The soil was modeled as soft clay, and its mechanical behavior was described by the Mohr-Coulomb model. The Material Point Method (MPM) was used to model the conductor-soil system. Three prescribed conductor velocities were simulated, and the resultant forces on the casing's outer surface were analyzed. The conductor displacement, reaction forces on the surface of the casing, and the soil's stress state were studied. For the conductor walls, the increase in driving velocity did not present significant differences. Higher velocities caused greater reaction forces at the conductor's tip. The conductor's tip experienced greater reaction forces than the side surface, suggesting that the tip shape exerts a significant influence on the total soil bearing capacity.

Keywords: Well construction, Soft clay, Self-weight, Installation.

1 Introduction

The oil industry has been striving each year to increase the safety of its operations. One way to enhance the reliability of a well is by understanding the variables behind its construction operations [1]. In this context, the start of a well in soft clays demands attention, as this type of soil provides low structural resistance and its modeling is full of uncertainties.

Among the main techniques for setting the conductor casing in deep and ultra-deep waters off the Brazilian coast are drilling followed by cementing, soil jetting, torpedo-based driving, and hammer driving [2–4].

Hammer driving presents some advantages over other techniques: it does not require the use of a drilling rig; driving does not remove soil from the environment, which avoids major soil disturbances; and it allows greater flexibility in changing the dimensions of the casing.

Hammer driving is comprised of three phases, namely, self-weight, suction, and hammering. In the first phase, the conductor is set exclusively by the gravitational force acting on it. Next, suction is applied around the casing. This process is based on the installation of suction anchors: a pipe with an open lower end and a closed upper end is wrapped around the conductor. A pressure differential is applied at the upper end, causing the casing to descend further. Finally, hammering is performed by a hydraulic hammer that transmits energy to the top of the conductor through the movement of a ram.

This work aims to understand how the displacement velocity of the conductor in the self-weight driving phase influences the stress distribution in the soil. For this purpose, a computational model using the Material Point Method (MPM) formulation was developed.

2 Methodology

The casing driving operation imposes significant displacement in the soil, which can cause excessive deformations in the numerical mesh. Deformations in the mesh can compromise the simulation results, making it necessary to abort the calculations. This problem can be overcome by using a meshless method or an adaptation of the Finite Element Method (FEM) such as the MPM.

2.1 Material Point Method

The MPM derives from the Particle in Cell Method (PIC), which is used in fluid mechanics. The MPM was extended to solids and initially used to model problems involving granular materials. With the success achieved in the implementation of the MPM, this method began to be used to model geomechanical problems.

The MPM avoids problems with large deformations in the numerical mesh by storing the deformations in a set of points within the elements of the numerical mesh, called Material Points (MP). The computational scheme of the MPM can be observed in Fig 1. At the beginning of the time increment, the information stored in the MPs is interpolated to the mesh nodes (a). Then, the governing equations of motion are solved at the mesh nodes (b). The nodal values are used to obtain information on velocity, stresses, and deformations in the MPs (c). The numerical mesh is reset at the end of each time increment, preventing the propagation of errors (d) [5].
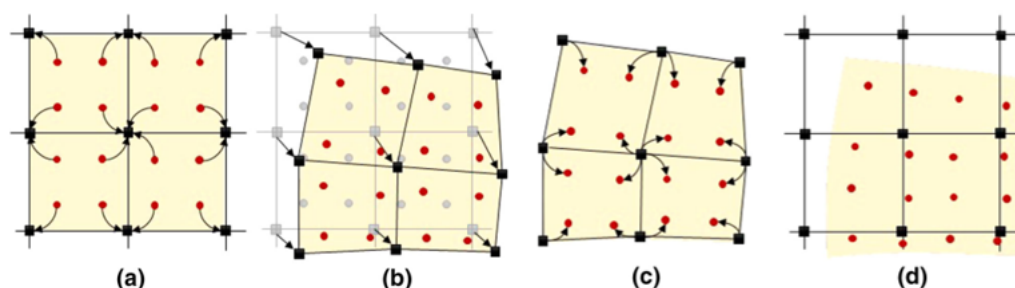
Figure 1. Computational scheme of MPM [5].

2.2 Contact algorithm

An accurate description of the contact properties between materials is of fundamental importance in problems involving soil penetration. One way to model the contact between materials is established by correcting the velocity difference between the bodies.

The model proposed by Bardenhagen et al. [6] is widely used in MPM-based simulations of geomechanical problems. In this formulation, the constitutive model of each particle is solved. The contact algorithm prevents interpenetration, permitting only separation and sliding. However, this model uses a fixed mesh, so only the particles move, requiring repeated mapping of the interface between materials to the nodes.

Al-Kafaji [7] introduced the concept of a moving mesh, which causes the mesh around the moving body to follow its displacement. This approach eliminates the necessity of recalculating the interface between materials, as it remains constant. The implementation of the moving mesh reduces inaccuracies in the calculation of the normal vectors required in the contact algorithm. Using the moving mesh with the contact algorithm allows better results.

Ceccato et al. [8] proposed an extension to the model introduced by Bardenhagen et al. [6] as the latter solely incorporates the Coulomb friction model, evaluating only the normal shear stress, which is unrealistic for undrained materials. The model proposed by Ceccato et al. [8] incorporates an adhesive contact law that accounts for the undrained shear stress.

This formulation considers that the individual velocities ($\mathbf{v_{k,A}}$, $\mathbf{v_{k,B}}$) of two bodies, referred to as A and B, and the combined velocity of the system ($\mathbf{v_{k,S}}$), can be computed by solving their respective equations of motion. For a contact node $\mathbf{k}$, $\mathbf{v_{k,A}}$ can be obtained using eq. 1 [8].

$$\bar{\mathbf{v}}_{\mathbf{k,A}} = \mathbf{v_{k,A}} + \mathbf{c_{k,norm}} + \mathbf{c_{k,tan}} \tag{1}$$

The interpenetration of materials is prevented by the normal correction component ($\mathbf{c_{k,norm}}$). The tangential correction component is represented by $\mathbf{c_{k,tan}}$. The material corrections are equivalent to applying the contact

forces $\mathbf{f_{k,norm}}$ (eq. 2) and $\mathbf{f_{k,tan}}$ (eq. 3).

$$\mathbf{f_{k,norm}} = \frac{m_{k,A}}{\Delta t}\mathbf{c_{k,norm}} \tag{2}$$

$$\mathbf{f_{k,tan}} = \frac{m_{k,A}}{\Delta t}\mathbf{c_{k,tan}} \tag{3}$$

The material corrections are controlled by the nodal mass $m_{k,A}$ and the time step increment (Δt). Therefore, in the event of interpenetration, these parameters can be modified to solve the problem.

The maximum contact force ($\mathbf{f_{k,tanmax}}$) depends on the friction coefficient (μ) and the adhesion factor (a). The maximum contact force can be calculated using eq. 4, in which A_k is the surface area of associated with node k.

$$\mathbf{f_{k,tanmax}} = (\mu|\mathbf{f}_{k,norm}| + aA_k)\mathbf{t_k} \tag{4}$$

3 Case study

3.1 Geometry and material properties

The geometry of this problem poses a challenge to its simulation. The casing has thin walls compared to its length dimension. Modeling the conductor as a hollow pipe would significantly increase the computational cost since the time increment is limited by the dimensions of the smallest mesh element, which would be the element of the pipe wall. Therefore, to avoid a prohibitive computational cost, the conductor casing was modeled with a closed end. The axisymmetry of the soil-conductor system was utilized, and only a slice of the system was modeled, as shown in Fig 2.
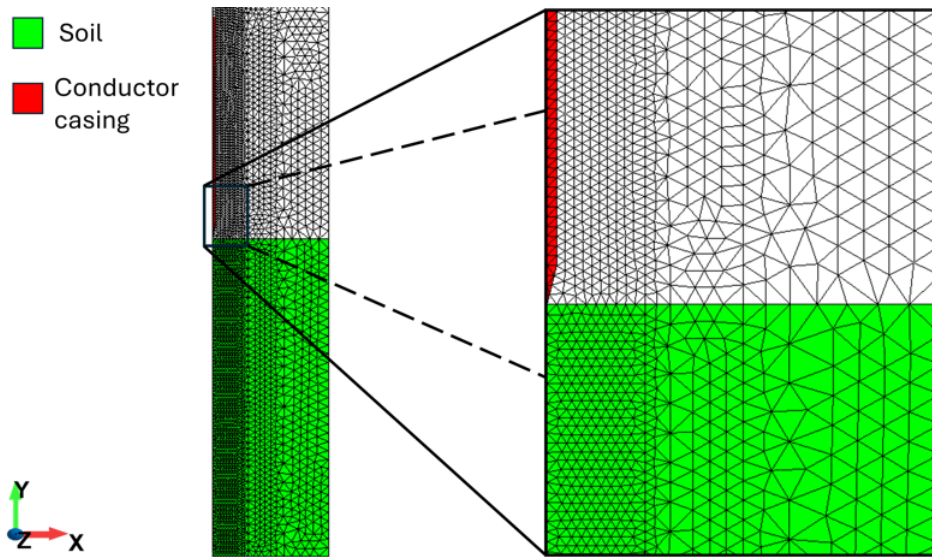
Figure 2. Model's geometry

The conductor was modeled as a rigid body since, when compared to the soil, the deformations it undergoes are very small. This consideration reduces the computational cost, for the Young's modulus has great influence in this parameter, increasing the stable time increment. Another simplification was related to the length of the conductor. The original dimensions of the structure were 36" (0.9144 m) in diameter (D_C) and 60 m long. As only the self-weight driving phase was simulated, the modeled conductor had a shorter length (35 m). However, the density of the conductor was adjusted so that its weight equaled the weight of a 60 m long casing with a density of 7860 kg/m³.

The soil has an equivalent diameter of 40 D_C and was modeled as a saturated material. The soil, which is composed of soft clay, was modeled using the Mohr-Coulomb constitutive model, with an effective cohesion of 9.27 kPa, friction angle of 36.29 deg, with both effective dilatancy angle and tensile strenght equals to zero. This constitutive model was chosen due to its simple calibration process, which can be done using in situ test data.

The soil properties were considered constant along the depth. For this purpose, an average of the properties obtained from the CPTu test was used. The soil was modeled as a saturated material and its properties are presented in Tab. 1. To model the contact between the conductor and the soil, a friction angle o f 0.423 rad and a adhesion factor of 4.64 kPa were used. The K0 procedure was used for stress initialization.

Table 1. Coefficients in constitutive relations

Parameter	Value	Unit
Density	1475.4	$\frac{kg}{m^3}$
Initial porosity	0.5833	-
Intrinsic permeability liquid	1.02e-9	
K0 value	0.961	-
Effective Poisson	0.49	-
Effective Young modulus	17.896	mPa

An unstructured numerical mesh was used to describe the model. The elements composing the soil were modeled with 6 MPs, as they require more attention compared to the conductor domain, which was modeled with 1 MP per element. The model consisted of 6,531 elements, 3,416 nodes, and 22,539 MPs. A computer with an Intel Core i5-9600K (3.70 GHz) processor, 16 GB of RAM, and Windows 11 (64-bit) was used to run the simulations.

3.2 Boundary conditions and parametric study

In self-weight driving, the casing is lowered at a controlled velocity until the soil resistance is sufficient to prevent further advancement. To represent this operation, the self-weight driving modeling was divided into two stages: displacement at a constant speed and then displacement only with gravitational acceleration. In this study, only the influence of velocity was examined.

The boundary conditions of the simulation can be observed in Fig 3. The lateral walls are restricted from moving along the horizontal axis. The top wall prevents vertical movements. The bottom wall restricts movement in all directions. Finally, the conductor casing has restricted horizontal movement, and a constant velocity is imposed on it. To analyze the influence of velocity, three models were constructed with velocities of 0.25 m/s, 0.5 m/s, and 1.0 m/s.
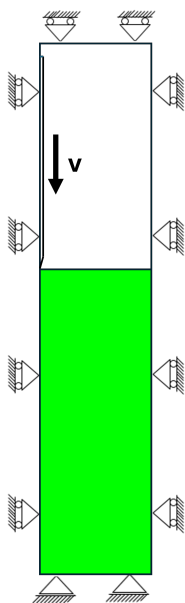
Figure 3. Model's boundary conditions.

3.3 Results

Two surfaces were defined in the conductor to study the soil reactions on the casing walls: one on the side wall and the other on the inclined part of the casing tip. In Fig. 4, it is possible to observe a comparison between the vertical component of the sum of the reaction forces acting on the surface of the conductor lateral face for the three analyzed cases.
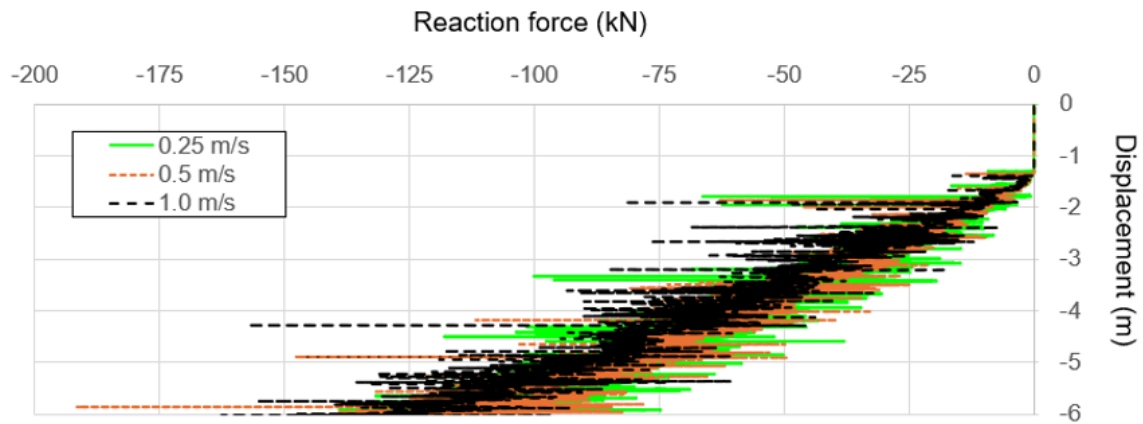
Figure 4. Reaction forces on the conductor casing lateral vs. displacement.

As can be seen, the reaction on the lateral walls was nearly the same for all three cases. The values obtained in the simulation, although following trends, exhibit oscillations around these lines. The oscillations can be caused by various reasons, one of them being insufficient dimensions of the soil geometry. The diameter or depth of the material may not be sufficient to allow the dissipation of waves within the medium [9]. Possible solutions to this problem involve changing the soil geometry, using damping in the material, and applying viscous or viscoelastic boundary conditions [10].

The reaction forces at the conductor tip can be observed in Fig 5. Unlike the comparison of reactions on the lateral wall, where the curves overlap, it is possible to note that higher conductor velocities will generate slightly higher reaction forces at its tip.
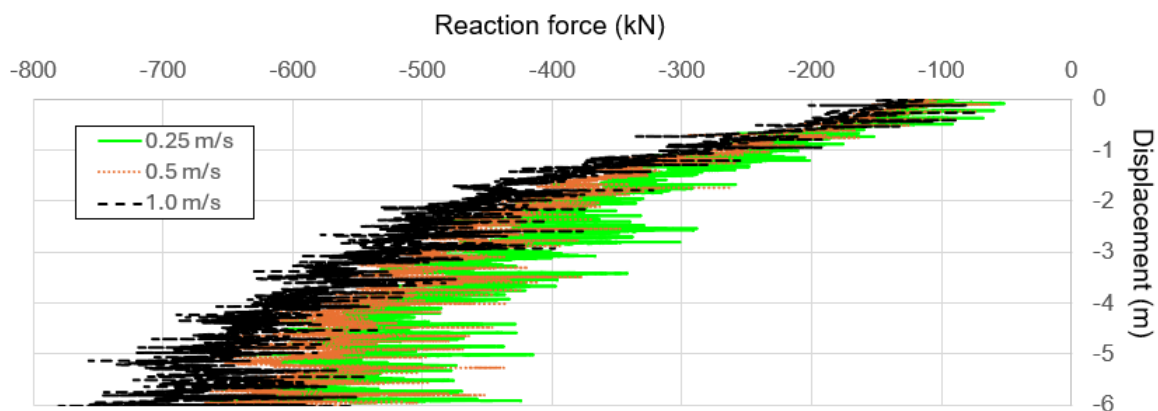
Figure 5. Reactions forces on the tip of conductor casing vs displacement.

As in the self-weight driving phase, the objective is to drive the casing as deep as possible so that the subsequent phases are smoother. This result shows that driving the conductor casing at a slower velocity during the self-weight phase will result in lower soil resistances at conductors tip. It is also worth noting that the magnitude of the reaction forces at the tip of the conductor is about four times that of the reaction forces on the conductor's wall.

The soil stresses in the simulation with a driving velocity of 0.25 m/s can be observed in Fig. 6. As described in the comparisons between the forces acting on the soil, the region closest to the tip of the conductor experiences

higher stresses in magnitude than casing side. However, the stress distribution exhibits some irregularities that can be noticed by the discrepancy in the transition of stress values between some neighboring elements. This irregularity may indicate poor discretization of the model. This problem can be solved by increasing the number of elements and/or the number of material points in the soil surrounding the conductor.
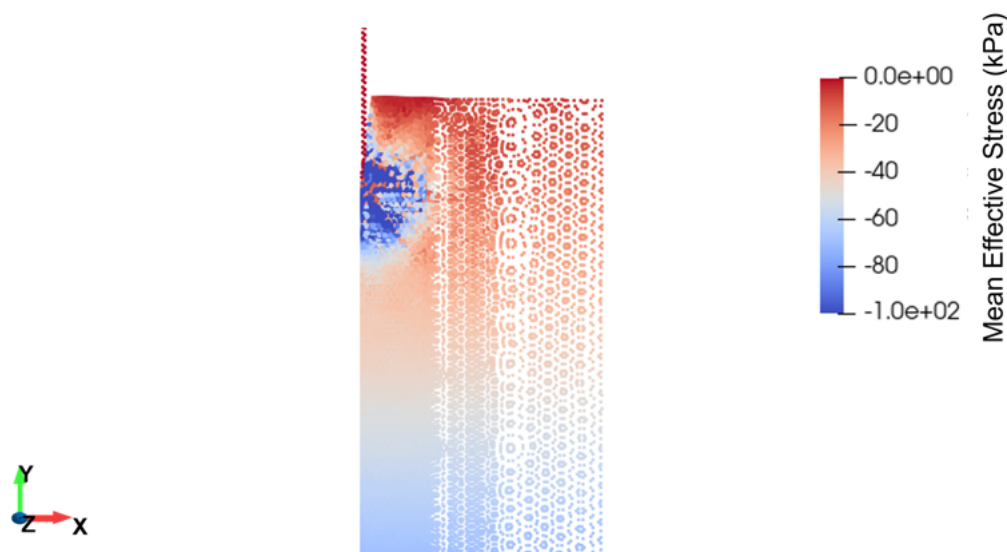
Figure 6. Soil's mean effective stress.

4 Conclusions

The self-weight driving phase was found to be slightly influenced by the vertical velocity of the conductor, with reaction forces on the conductor's tip being more impacted than its walls. Higher velocities resulted in larger reaction forces on the soil near the conductor's tip, which is undesirable during this stage of the casing installation. The reactions forces exhibited oscillations, which may have been influenced by boundaries located too close to the conductor. Future studies are suggested to assess the influence of geometry and the use of damping formulations in the soil. The soil stress distribution suggests the need to increase the discretization of the soil, either by increasing the number of elements or material points. The conductor tip was found to have some influence on the reaction forces. Therefore, future studies are suggested to evaluate different angles of inclination for the apex of the tip, in order to make the results closer to those of a simulation of an open conductor.

Authorship statement. The authors hereby confirm that they are the sole liable persons responsible for the authorship of this work, and that all material that has been herein included as part of the present paper is either the property (and authorship) of the authors, or has the permission of the owners to be included here.

References

[1] *Real-Time and Wireless Monitoring of Wellhead and Conductor Fatigue*, volume Day 2 Tue, August 23, 2016 of *IADC/SPE Asia Pacific Drilling Technology Conference and Exhibition*, 2016.
[2] *Conductor Batch Drilling Rig Time Optimization by Cementing with Low-Density Low-Temperature Fast Setting Cement*, volume Day 2 Tue, July 28, 2020 of *SPE Latin America and Caribbean Petroleum Engineering Conference*, 2020.
[3] *Investigation of a Jetted Conductor Failure in a Pre-Salt Well and Lessons Learned*, volume Day 1 Mon, May 01, 2023 of *OTC Offshore Technology Conference*, 2023.

[4] *Torpedo Base - A New Conductor Installation Process*, volume All Days of *OTC Offshore Technology Conference*, 2005.

[5] F. Ceccato and P. Simonini. Numerical study of partially drained penetration and pore pressure dissipation in piezocone test. *Acta Geotechnica*, vol. 12, pp. 195–209, 2017.

[6] S. Bardenhagen, J. Brackbill, and D. Sulsky. The material-point method for granular materials. *Computer methods in applied mechanics and engineering*, vol. 187, n. 3-4, pp. 529–541, 2000.

[7] I. K. Al-Kafaji. *Formulation of a dynamic material point method (MPM) for geomechanical problems*. Citeseer, 2013.

[8] F. Ceccato, L. Beuth, and P. Simonini. Adhesive contact algorithm for mpm and its application to the simulation of cone penetration in clay. *Procedia Engineering*, vol. 175, pp. 182–188, 2017.

[9] L. Li and I. Kao. Damped Vibration Response of An Axially Moving Wire Subject to An Oscillating Boundary Condition and the Application to Slurry Wiresaws. *Journal of Vibration and Acoustics*, vol. 143, n. 5, pp. 051002, 2021.

[10] P. C. Do, P. J. Vardon, J. L. González Acosta, and M. A. Hicks. Implementing dynamic boundary conditions with the material point method. In *International Conference of the International Association for Computer Methods and Advances in Geomechanics*, pp. 221–228. Springer, 2022.